The Cryosphere Discuss., https://doi.org/10.5194/tc-2019-55
Manuscript under review for journal The Cryosphere
Discussion started: 25 March 2019


The Cryosphere Discussions

# Glacier thickness estimations of alpine glaciers using data and modeling constraints

Lisbeth Langhammer[1]
Melchior Grab[1,2]
Andreas Bauder[2]
Hansruedi Maurer[1*]

[1] Institute of Geophysics, ETH Zurich, Switzerland
[2] Laboratory of Hydraulics, Hydrology and Glaciology (VAW), ETH Zurich, Switzerland
[*] Corresponding author (*hansruedi.maurer@erdw.ethz.ch* )

## Abstract

Advanced knowledge of the ice thickness distribution within glaciers is of fundamental importance for several purposes, such as water resource management and studying the impact of climate change. Ice thicknesses can be modeled using ice surface features, but the resulting models can be prone to considerable uncertainties. Alternatively, it is possible to measure ice thicknesses, for example, with ground-penetrating-radar (GPR). Such measurements are typically restricted to a few profiles, with which it is not possible to obtain spatially unaliased subsurface images. We developed the Glacier Thickness Estimation algorithm (GlaTE), which optimally combines modeling results and measured ice thicknesses in an inversion procedure to obtain overall thickness distributions. Properties and benefits of GlaTE are demonstrated with three case studies performed on different types of alpine glaciers. In all three cases, subsurface models could be found that are consistent with glaciological modeling and GPR data constraints. Since acquiring GPR data on glaciers can be an expensive endeavor, we additionally employed elements of sequential optimized experimental design (SOED) for determining cost-optimized GPR survey layouts. The calculated benefit-cost curves indicate that a relatively large amount of data can be acquired, before redundant information is collected with any additional profiles and it becomes increasingly expensive to obtain further information. Only at one out of the three test sites this level was reached.

The Cryosphere Discuss., https://doi.org/10.5194/tc-2019-55
Manuscript under review for journal The Cryosphere
Discussion started: 25 March 2019


The Cryosphere Discussions

# 1 Introduction

Estimating the amount of the glacier ice around the globe is crucial, for example, for sea-level predictions, securing fresh water recourses, designing hydropower facilities in high-alpine environments, and predicting the occurrence of glacier-related natural hazards. For estimating the overall glacier ice mass and its local distribution, (i) knowledge of the glacier outline, (ii) its surface topography and (iii) the underlying bedrock topography is required. The first two quantities can be observed with aerial and satellite imagery, but the bedrock topography is more difficult to determine.

The conceptually simplest option includes drilling boreholes through the glacier ice (e.g., Iken, 1988). This approach offers ground-truth information, but only a very sparse observation grid can be obtained with realistic efforts. Therefore, geophysical methods have been employed for obtaining more detailed information. Due to the very high electrical resistivity of glacier ice and the relatively high electromagnetic impedance contrast between ice and bedrock material, ground-penetrating-radar (GPR) techniques, also referred to as radio-echo-sounding (RES), have been the primary choice for such investigations (e.g., Evans, 1963). GPR data can either be acquired ground-based (e.g., Watts and England, 1976), or, more efficiently, using fixed-wing airplanes (e.g., Steinhage et al., 1999) or helicopters (e.g., Rutishauser et al., 2016).

Despite the powerful capabilities of modern GPR acquisition systems, it is still beyond any practical limits to acquire spatially un-aliased 3D data sets. GPR data are therefore collected only along a sparse network of profiles, which leaves considerable uncertainties in the regions between the profiles.

To address this problem, glaciological modeling techniques have been established to relate observable surface parameters to the thickness distribution of ice. One of the earliest concepts was published by Nye (1952). He established a simple relationship between the surface slope and ice thickness. During the past decades, more sophisticated ice thickness modeling techniques have emerged rapidly. Various glaciological constraints, such as mass conservation and/or the relation between basal shear stress and ice thickness, were considered (e.g., Farinotti et al., 2009;Huss and Farinotti, 2012;Clarke et al., 2013;Linsbauer et al., 2012;Morlighem et al., 2011). See Farinotti et al. (2017) for a more complete review of most of the approaches published to date.

Due to inaccuracies of the observed data (GPR measurements, surface topography, etc.) and/or inadequacies of the modeling approaches, modeled ice thicknesses cannot be expected to be perfect. This can be considered by formulating ice thickness estimation as an optimization problem, in which the discrepancies between observed and predicted data are minimized (e.g., Morlighem et al., 2014). In this contribution, we follow an approach similar to Morlighem et al. (2014), but with a different implementation. We introduce the general framework of Glacier Thickness Estimation (GlaTE), with which modeling and data constraints can be combined in an appropriate fashion. After introducing the underlying theory, we demonstrate the performance of the GlaTE inversion procedure with three case studies. In the second part of the paper, we employ elements of GlaTE to address the experimental design problem. Here, we seek a measured data set that offers maximum information content at minimal costs. For that purpose, we consider sequentially optimized experimental design (SOED) techniques (e.g., Maurer et al., 2017). The paper concludes with a critical review of potential problems and shortcomings of GlaTE and the associated SOED procedures, and we outline options to address these issues and propose useful extensions of the methodology.

## 2 GlaTE inversion algorithm

### 2.1. Theory

The basic idea of GlaTE inversions is to combine observable data with glaciological modeling constraints, whereby it is attempted to consider appropriately the uncertainties associated with both types of information. All constraints are formulated, such that they can be integrated into a single system of equations, which can be solved with an appropriate solver.

The first type of constraints includes the GPR data. They can be written in the form of

(1) $$\mathbf{G}\mathbf{h}^{\mathbf{est}} = \mathbf{h}^{\mathbf{GPR}} ,$$

where $\mathbf{h}^{\mathbf{est}}$ is a vector including the unknown (*est*imated) ice thicknesses at M locations (typically defined on a regular grid *R* on a glacier), and **G** is a $N^{GPR} \times M$ matrix with ones in its main diagonal and zeros everywhere else ($N^{GPR}$ = number of available GPR data points, $M$ = number of elements in $\mathbf{h}^{\mathbf{est}}$). The vector $\mathbf{h}^{\mathbf{GPR}}$ of length $N^{GPR}$ includes the GPR-based thickness estimates. Since the GPR data usually do not coincide with the grid points of *R*, the values $\mathbf{h}^{\mathbf{GPR}}$ are obtained by interpolating or extrapolating the GPR data to the nearest grid points of *R*.

Next, we consider glaciological modeling constraints. In principle, any of the algorithms proposed in the literature can be employed. Here, we follow closely the approach described in Clarke et al. (2013). Input data include a digital terrain model (DTM, defined on *R*) and the glacier outline.

First, the glacier area is subdivided into so-called flowsheds using the Matlab TOPO-Toolbox (Schwanghart and Kuhn, 2010). The subsequent procedure is applied to each flowshed individually (see comments in Clarke et al. (2013) for more information on the flowshed subdivision).

Next, the apparent mass-balance, defined as

(2) $$\tilde{\mathbf{b}} = \dot{\mathbf{b}} - \frac{\partial \mathbf{h}}{\partial t} ,$$

The Cryosphere Discuss., https://doi.org/10.5194/tc-2019-55
Manuscript under review for journal The Cryosphere
Discussion started: 25 March 2019


with $\dot{\mathbf{b}}$ being the mass balance rate, and $\frac{\partial \mathbf{h}}{\partial t}$ the thickness change rate, is either determined by measuring $\dot{\mathbf{b}}$ and $\frac{\partial \mathbf{h}}{\partial t}$, or computed via the condition

(3) $$\int_{\Omega_G} \tilde{\mathbf{b}} = 0 ,$$

where $\Omega_G$ denotes the glacier area (see Farinotti et al. (2009) for more details). In a next step, the flowsheds are partitioned into a prescribed number of elevation zones $D_i$ ($i = 1 \ldots$ *number of elevation zones*), for which the ice discharge $Q_i$ through its lower boundary is computed using

(4) $$Q_i = \int_{\Omega_{D_i}} \tilde{\mathbf{b}} ,$$

where $\Omega_{D_i}$ is the area of zone $D_i$. Following Clarke et al. (2013), the basal shear stress $\tau$ can then be obtained via the relationship

(5) $$\boldsymbol{\tau} = \left[ \frac{(n+2)\rho g \sin(\phi)^2 \xi \mathbf{q}}{2A} \right]^{1/(n+2)}$$

The parameters $n$, $\rho$, g and $A$ denote the exponent of Glen's flow law, ice density, gravity acceleration and creep rate factor, respectively (e.g., Cuffey and Patterson, 2010). The factor $\xi$ denotes the creeping contribution (relative to basal sliding) to the ice flux $(0 < \xi < 1)$, and $\mathbf{q}$ is the specific ice discharge $q_i = \overline{Q}_i / l_i$, where $l_i$ is the length of the lower boundary of $D_i$, and $\overline{Q}_i$ is the average of $Q_i$ within $D_i$. Likewise, the angle $\phi$ represents the surface slope averaged along the lower boundary of $D_i$.

As outlined in Kamb and Echelmeyer (1986), the physics of ice flow can be incorporated into the modeling procedure by applying "longitudinal averaging" of the shear stress (i.e., along the flow direction). We apply this procedure to the results obtained with Equation (5). Finally, the ice thicknesses $\hat{\mathbf{h}}^{\mathbf{glac}}$ (*glac* stands for glaciological modeling constraints) are obtained using

(6) $$\hat{\mathbf{h}}^{\mathbf{glac}} = \frac{\boldsymbol{\tau}^*}{\rho g \sin(\theta)} ,$$

where $\boldsymbol{\tau}^*$ denotes the basal shear stress after longitudinal averaging.

Some of the parameters in Equation (5) may be subject to considerable uncertainties. For example, the parameter $\xi$ is often poorly known, and it is not guaranteed that the values of the parameters $A$ and $n$, usually taken from the literature, are accurate. Typically, $n$ is reasonable well constrained, but A can vary over orders of magnitudes. Therefore, the overall magnitudes of $\hat{\mathbf{h}}^{\mathbf{glac}}$ may be significantly over- or under-estimated. This can be considered with an additional factor $\alpha_{GPR}$, yielding

(7) $$\mathbf{h}^{\mathbf{glac}} = \alpha_{GPR} \hat{\mathbf{h}}^{\mathbf{glac}} .$$

$\alpha_{GPR}$ can be computed with an optimization procedure that minimizes $\left| mean\left( \mathbf{h}^{\mathbf{GPR}} - \alpha_{GPR} \hat{\mathbf{h}}^{\mathbf{glac}} \right) \right|$.

The correction factor $\alpha_{GPR}$ accounts for some inadequacies of Equation (5), but it is still possible that there are systematic differences between $\mathbf{h}^{\mathbf{GPR}}$ and $\mathbf{h}^{\mathbf{glac}}$. To avoid the resulting inconsistencies, we consider not the absolute values $\mathbf{h}^{\mathbf{glac}}$, but the spatial gradients $\nabla \mathbf{h}^{\mathbf{glac}}$ as glaciological constraints, resulting in

(8) $$\mathbf{L}\mathbf{h}^{\mathbf{est}} = \nabla \mathbf{h}^{\mathbf{glac}} ,$$

where **L** is a difference operator of dimension $M \times M$.

Further constraints can be imposed via the glacier boundaries that can be determined from aerial or satellite images or ground observations. They are considered in the form of the equation

(9) $$\mathbf{B}\mathbf{h}^{\mathbf{est}} = 0 ,$$

where **B** is a $M \times M$ matrix with ones at appropriate places in its main diagonal.

Depending on the discretization of the glacier models (i.e., the discretization of $R$), the constraints described above, may allow the resulting system of equations to be solved unambiguously. However, in most cases, there will be still a significant underdetermined component, that is, there will be many solutions that explain the data equally well. This requires regularization constraints to be applied (e.g., Menke, 2012). A common strategy for regularizing such problems is to follow the Occam's principle, which identifies the "simplest" solution out of the many possible solutions (Constable et al., 1987). Here, we define "simplicity" in terms of structural complexity, that is, we seek a smooth model. This can be achieved via a set of smoothing equations of the form

(10) $$\mathbf{S}\mathbf{h}^{\mathbf{est}} = 0 ,$$

where **S** is a $M \times M$ smoothing matrix.

The Cryosphere Discuss., https://doi.org/10.5194/tc-2019-55
Manuscript under review for journal The Cryosphere
Discussion started: 25 March 2019

The Cryosphere Discussions

All the constraints can now be merged into a single system of equations

$$(11)\quad \begin{pmatrix} \lambda_1 \mathbf{G} \\ \lambda_2 \mathbf{L} \\ \lambda_3 \mathbf{B} \\ \lambda_4 \mathbf{S} \end{pmatrix} \mathbf{h}^{\mathbf{est}} = \begin{pmatrix} \lambda_1 \mathbf{h}^{\mathbf{GPR}} \\ \lambda_2 \nabla \mathbf{h}^{\mathbf{glac}} \\ 0 \\ 0 \end{pmatrix},$$

where the parameters $\lambda_1$ to $\lambda_4$ allow a weighting according to the confidence into individual contributions. Parameter $\lambda_3$ is not critical and can be fixed to an appropriate value (e.g., 1.0). The magnitudes of the remaining three parameters must be chosen, such that the system of equations in (11) is solvable. However, it also needs to be considered that all the constraints related to $\lambda_1$, $\lambda_2$ and $\lambda_4$ may be subject to significant inaccuracies. It is difficult to predict the accuracy of the modeling constraints and to judge the appropriateness of the smoothing constraints, but the accuracy of the GPR data constraints, subsequently denoted as $\boldsymbol{\varepsilon}^{\mathbf{GPR}}$, can usually be quantified. Therefore, $\lambda_1$, $\lambda_2$ and $\lambda_4$ have to be chosen, such that the discrepancy of the GPR data $\left(\left\|\mathbf{G}\mathbf{h}^{\mathbf{est}} - \mathbf{h}^{\mathbf{GPR}}\right\|\right)$ is of the order of $\boldsymbol{\varepsilon}^{\mathbf{GPR}}$, and the GPR data are thus neither under- nor over-fitted. We have implemented this by choosing the magnitudes of $\lambda_1$, $\lambda_2$ and $\lambda_4$, such that a prescribed percentage of the GPR data (e.g., 95%) satisfies $\left\|\mathbf{G}\mathbf{h}^{\mathbf{est}} - \mathbf{h}^{\mathbf{GPR}}\right\| < \boldsymbol{\varepsilon}^{\mathbf{GPR}}$.

This can be achieved with different strategies. One option is to fix $\lambda_2$ and $\lambda_4$, and to vary $\lambda_1$ until the condition, mentioned above, is met. Alternatively, it is possible to fix the pairs $\lambda_1/\lambda_4$ or $\lambda_1/\lambda_2$ and to vary $\lambda_2$ or $\lambda_4$. Choice of the most appropriate strategy depends on the uncertainties associated with the individual contributions in Equation (11) .

The dimension of the system of equations in (11) can be very large, but the matrices **G**, **L**, **B** and **S** are all extremely sparse. Therefore, sparse matrix solvers, such as LSQR (Paige and Saunders, 1982) can solve such systems efficiently for $\mathbf{h}^{\mathbf{est}}$.

## 2.2 Performance tests

For testing the GlaTE inversion algorithm, we investigated glacier ice thickness at three sites in the Swiss Alps (Figure 1). The first site is Morteratschgletscher (Figure 1a). Lying at altitudes between 2050 and 4000 m a.s.l. (Zekollari et al., 2013), the glacier has a typical valley-glacier shape and is located in the Engadin region of Switzerland. In 2015, the tributary glacier Vadret Pers in the east detached from the main trunk of Morteratschgletscher, but we continue to treat both glaciers as a connected system, since

The Cryosphere Discuss., https://doi.org/10.5194/tc-2019-55
Manuscript under review for journal The Cryosphere
Discussion started: 25 March 2019


the last available outline of the glaciers in 2015 shows the remnant of the former connection. In 2010, the glacier system covered an area of ≈ 15 km$^2$, and it had a length of ≈ 7.4 km.

The second site, Glacier Plaine Morte (2400-3000 m a.s.l., (Figure 1b), is the largest plateau glacier in the European Alps (Huss et al., 2013). The surface slope is shallow with slope angles less than 4° and a short glacier tongue draining towards the North.

The third site is a cluster of small valley flank and cirque-type glaciers on the eastern flank of the Matter valley (Figure 1c) below the Dom peak. From North to South, the glaciers are named Hohbärggletscher, Festigletscher, Kingletscher and Weingartengletscher. The Hohbärggletscher is the largest (2800-4500 m a.s.l.) and longest of the group.

For all sites, the recorded GPR profiles are shown in Figure 1. The GPR data are a composite of several campaigns. Most of the data were recorded with the dual polarization system AIR-ETH (Langhammer et al., 2018). On the Glacier Plaine Morte, a grid of profiles was acquired in 2016, and on the Morteratschgletscher and in the Dom Region in 2017. The data were processed as described in Grab et al. (2018), and the bedrock depths and the corresponding ice thicknesses were obtained from the migrated GPR images.

As input data for the glacier models, surface topography and an outline of the individual glaciers was required. As surface topography, we used the swissALTID3D (DTM, Digital Terrain Model Release 2017 © swisstopo (JD100042)). The most recent version covering the individual glaciers was extracted and down-sampled to 10 m resolution. The outline represents the extension of the glacier in 2015-2016. DTM and glacier outlines are displayed in Figure 1.

The Cryosphere Discuss., https://doi.org/10.5194/tc-2019-55
Manuscript under review for journal The Cryosphere
Discussion started: 25 March 2019



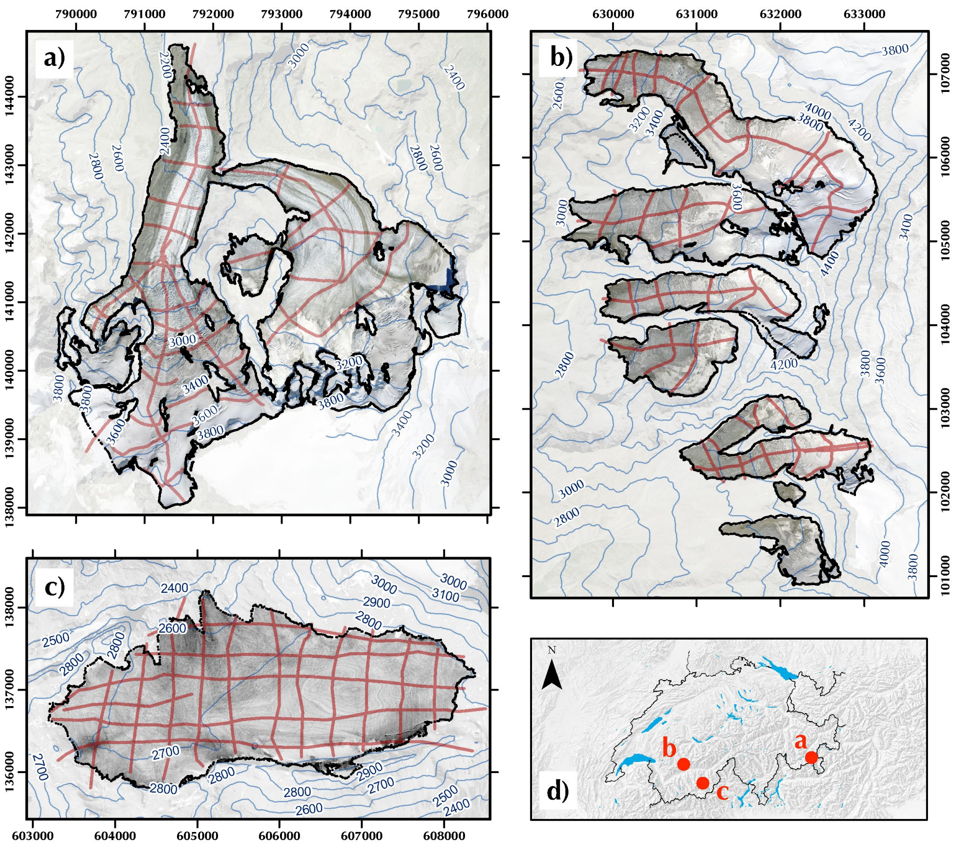


*Figure 1: Satellite images and surface topography isolines of the glaciers investigated. (a) Morteratschgletscher, (b) Glacier Plaine Morte and (c) Dom region. The Swiss map in the bottom right panel indicates the locations of the glaciers. GPR profiles acquires are shown in red. Orthophotos © 2017 swisstopo (JD100042). Coordinate system: CH1903.*

Before applying GlaTE inversions to all field sites, we tested the different options for determining $\lambda_1$, $\lambda_2$ and $\lambda_4$, using the data from Morteratschgletscher. Figure 2 shows the ice thicknesses distributions, (i) when only glaciological constrains are applied ($\mathbf{h}^{\mathrm{glac}}$, Figure 2a), and (ii) when only GPR constraints are considered ($\mathbf{h}^{\mathrm{GPR}}$, Figure 2b). In the latter case, the thicknesses are obtained by natural neighbor interpolation from the GPR data. Since no extrapolation was performed, not all glacierized regions have an ice thickness estimate. Both images exhibit increased thicknesses in the western glacier, but only the glaciological constraints indicate an overdeepening in the eastern one, thereby indicating that the two models are inconsistent.

The Cryosphere Discuss., https://doi.org/10.5194/tc-2019-55
Manuscript under review for journal The Cryosphere
Discussion started: 25 March 2019

The Cryosphere Discussions
Open Access
EGU

Figure 3 shows the results of the GlaTE inversions using either prescribed $\lambda_1/\lambda_4$ (Figure 3a), $\lambda_1/\lambda_2$ (Figure 3c) or $\lambda_2/\lambda_4$ (Figure 3e) pairs. The corresponding difference plots (Figure 3b, d and f) refer to the deviation of the obtained thickness results compared with the thickness calculated with the glaciological approach. We varied the $\lambda_2$ and $\lambda_4$ parameters by starting with very high values of 50, and by decreasing them successively until 95% of the GPR data met the condition $\left\|\mathbf{Gh}^{\mathbf{est}} - \mathbf{h}^{\mathbf{GPR}}\right\| < \boldsymbol{\varepsilon}^{\mathbf{GPR}}$, where $\boldsymbol{\varepsilon}^{\mathbf{GPR}}$ was estimated to be 5 m. In contrast, we started with a low value of 0.02 for variable $\lambda_1$, and increased it successively until 95% of the data were fitted within the error $\boldsymbol{\varepsilon}^{\mathbf{GPR}}$. Table 1 summarizes the prescribed and estimated $\lambda$ values.

All three inversion strategies (i.e., either varying $\lambda_2$, $\lambda_4$ or $\lambda_1$) yielded comparable results. Although the difference plots with respect to the glaciological model exhibit considerable differences (Figures 3b, 3d and 3f), the general shapes obtained with the glaciological constraints were well preserved in regions where the GPR data coverage was poor. From this first test, we conclude that (i) the GlaTE inversion approach works well, and (ii) that the strategy by which the values of $\lambda$ are chosen is not critical.

| **Inversion type** | $\lambda_1$ | $\lambda_2$ | $\lambda_3$ | $\lambda_4$ | **Figures** |
|---|---|---|---|---|---|
| $\lambda_1/\lambda_4$ fixed | 1 | 0.78 | 1 | 10 | 3a, 3b<br>4c, 4d |
| $\lambda_1/\lambda_2$ fixed | 1 | 1 | 1 | 7.8 | 3c, 3d |
| $\lambda_2/\lambda_4$ fixed | 1.28 | 1 | 1 | 10 | 3e, 3f |
| $\lambda_1/\lambda_4$ fixed | 1 | 1.56 | 1 | 2 | 4a, 4b |
| $\lambda_1/\lambda_4$ fixed | 1 | 0.00 | 1 | 50 | 4e, 4f |

*Table 1: Weighting parameters $\lambda$ employed for the GlaTE inversions shown in Figures 3 and 4. Numbers marked red indicate varying parameters.*

It is instructive to study the effects of an overly small or large (fixed) $\lambda_4$ value. As shown in Table 1, we employed a prescribed value of 10 for $\lambda_4$. This value was chosen by trial and error. There was a range of $\lambda_4$ values around 10 that yielded similar results (not shown). Choosing very low or high $\lambda_4$ values (i.e., $\lambda_4 = 2$ resp. $\lambda_4 = 50$) has a detrimental effect on the results, as shown in Figure 4. For $\lambda_4 = 2$, the inversion fits the ice thicknesses obtained from the GPR data only along the profile lines and maintains the glaciological modeling results in the remaining areas. This produces artificial features in the thickness map (Figure 4a). In contrast, $\lambda_4 = 50$ produces overly smooth images, which is obscuring small-scale variations from the glaciological constraints in regions

The Cryosphere Discuss., https://doi.org/10.5194/tc-2019-55
Manuscript under review for journal The Cryosphere
Discussion started: 25 March 2019


poorly covered by GPR data (Figure 4e). It is also noteworthy that even with $\lambda_2 = 0$ only approx. 70% of the discrepancies $\left\| \mathbf{Gh}^{\mathrm{est}} - \mathbf{h}^{\mathrm{GPR}} \right\|$ were below $\boldsymbol{\varepsilon}^{\mathrm{GPR}}$ (Figure 5e).

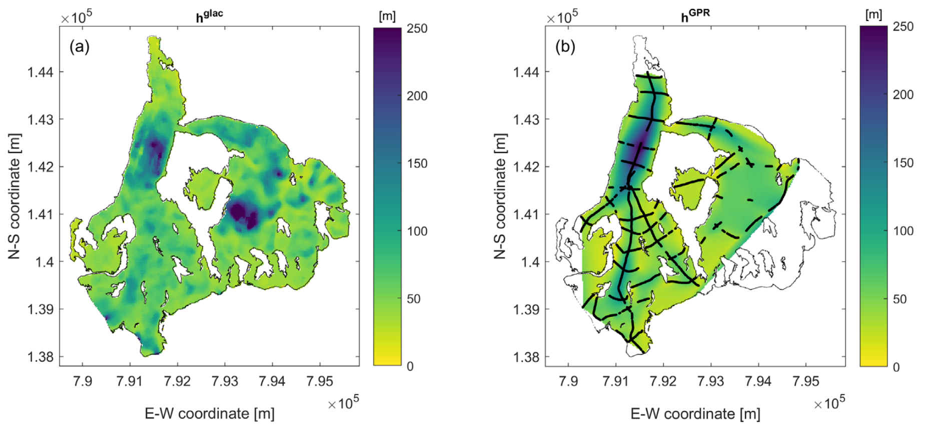


*Figure 2: Results from Morteratschgletscher only using (a) glaciological constraints and (b) GPR constraints. Colors indicate ice thickness. Available thickness data obtained from GPR profiles are marked with black lines.*

The Cryosphere Discuss., https://doi.org/10.5194/tc-2019-55
Manuscript under review for journal The Cryosphere
Discussion started: 25 March 2019


The Cryosphere Discussions
Open Access

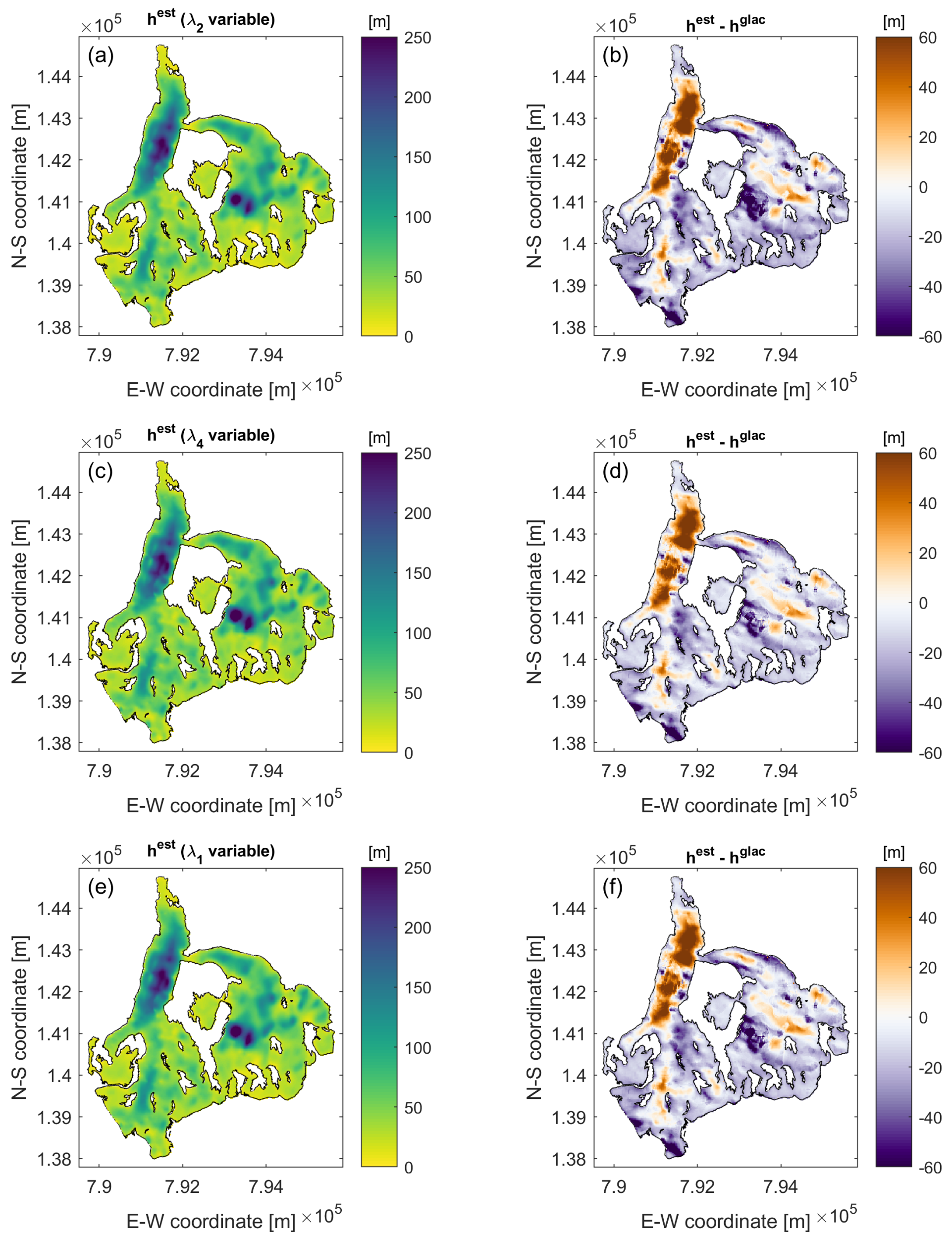


*Figure 3: Results from Morteratschgletscher using different strategies for choosing weighting parameters λ (see text for more explanations). Left panels show ice thickness distributions and right panels show differences to glaciological model without GPR constraints (Figure 2a).*

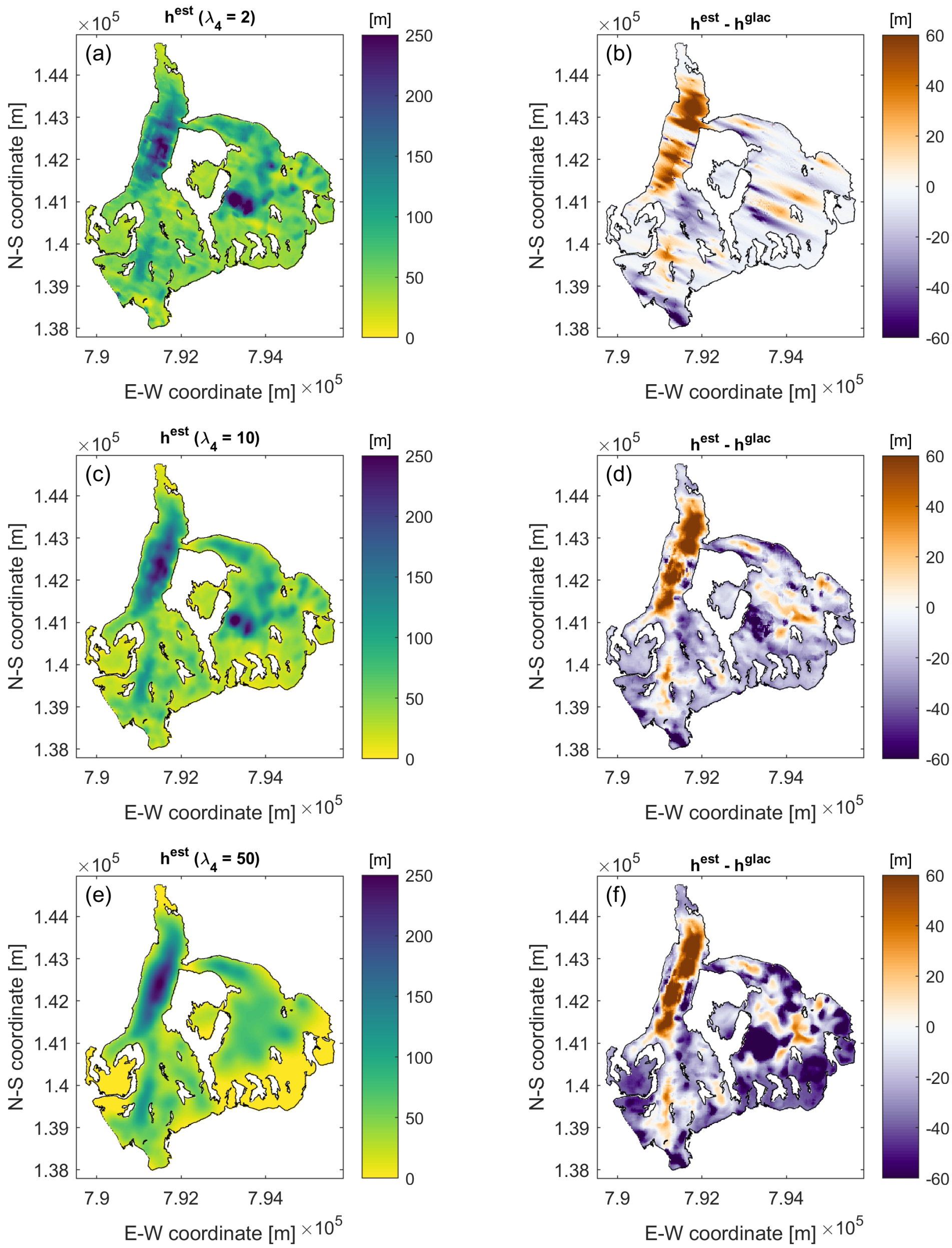


Figure 4: Results from Morteratschgletscher using fixed $\lambda_1$ and $\lambda_4$ values and varying $\lambda_2$. (a) and (b) are the results for $\lambda_4 = 2$, (c) and (d) for $\lambda_4 = 10$ and (e) and (f) for $\lambda_4 = 50$. Left panels show ice thickness distributions and right panels show differences to glaciological model without GPR constraints (Figure 2a).

The Cryosphere Discuss., https://doi.org/10.5194/tc-2019-55
Manuscript under review for journal The Cryosphere
Discussion started: 25 March 2019


The Cryosphere Discussions
Open Access
EGU

In the following, we consider only the scheme in which $\lambda_1/\lambda_2$ is kept fixed $(\lambda_1 = 1, \lambda_2 = 1)$, and $\lambda_4$ is varied for analyzing the Glacier Plaine Morte and the Dom region data. The results are shown in Figures 5 and 6. For the Glacier Plaine Morte, the glaciological model suggests a deep isolated trough slightly east of the center (Figure 5a). This is not supported by the GPR data, which rather indicate a larger E-W oriented elongated zone of increased thickness (Figure 5b). Such a feature is also contained in the GlaTE inversion results (Figure 5c). Furthermore, the glaciological model in Figure 5a overestimates the ice thickness in the northeastern part of the glacier.

Results from the Dom region show a relatively good match between the glaciological model (Figure 6a) and the GlaTE inversion result (Figure 6c). The glaciological model tends to underestimate the maximum thickness in the center of the glacier tongues, and to overestimate the thickness towards the edges (Figure 6d). The isolated trough structures (ice thickness > 200 m) in the northernmost glacier in the glaciological model (Figure 6a) are only partially supported by the GPR data (Figure 6b) and the GlaTE inversion (Figure 6c). In the southernmost Weingartengletscher, no data constraints exist (Figure 6b). The non-zero differences in this part (Figure 6d) are the result of the smoothing constraints. Here, the thickness estimates from the glaciological model are thus more trustworthy.

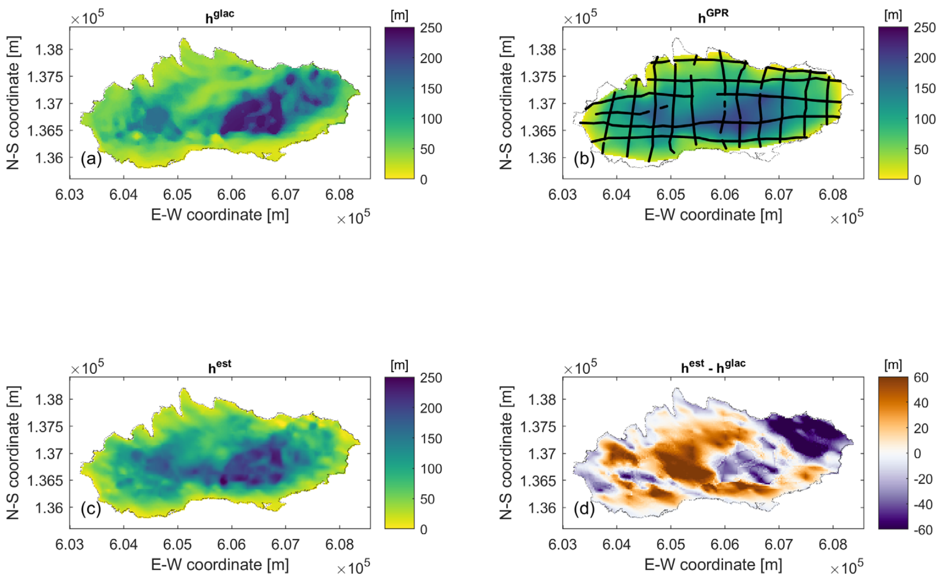


*Figure 5: Results from Plaine Morte Glacier. (a) only glaciological constraints, (b) only GPR constraints (available thickness data from GPR profiles marked with black lines), (c) GlaTE inversion, (d) difference between GlaTE inversion and glaciological model.*

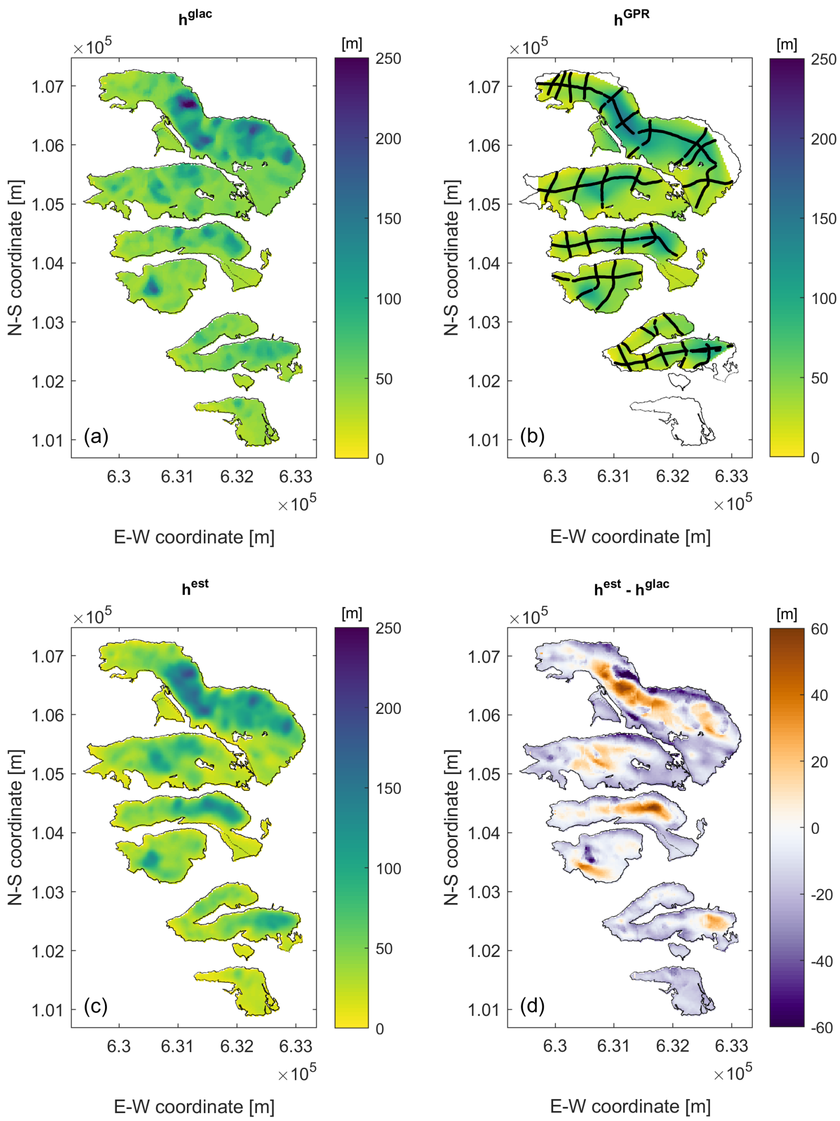


*Figure 6: Results from the Dom region. (a) only glaciological constraints, (b) only GPR constraints (available thickness data from GPR profiles marked with black lines), (c) GlaTE inversion, (d) difference between GlaTE inversion and glaciological model.*

# 3 Optimized experimental design using GlaTE inversion

All the investigations, described in Section 2, were based on existing GPR data. Their experimental layouts were designed heuristically using experience from prior surveys. Once a glacier model has been established, one may realize that another GPR survey layout may have provided better information. Therefore, a dense survey grid, as employed for 3D seismic reflection campaigns for hydrocarbon exploration for example (e.g., Vermeer, 2003) would be the best choice. This, however, would exceed by far the budgets typically available for glacier investigations.

Optimizing the glaciological constraints with only a limited number of GPR data is a chicken-and-egg problem: identifying the most useful GPR data to be added would require knowledge on where the true ice thickness distribution deviates most from the distribution in the glaciological model, but this would require advanced prior knowledge about the ice thickness that one wants to measure. The problem can be tackled nevertheless by making some specific assumptions (see below).

With our investigations, we address the following questions.

1. Was the experimental geometry and the amount of data acquired in the three investigation areas adequate?
2. Do better experimental layouts exist for constraining the ice thicknesses in a cost-optimized manner?
3. Can some general recommendations be made for designing helicopter-borne GPR surveys on glaciers?

Due to the lack of knowledge on the true ice thicknesses, we assumed that the GlaTE inversion results, shown in Figures 3, 5 and 6 are a good proxy for the actual thickness distributions. Without GPR data, the state of knowledge is represented by the glaciological model (Figures 2a, 5a and 6a). For these models, only 16% (Morteratsch), 10% (Plaine Morte) and 23% (Dom) of the GPR data constraints satisfy the condition $\left\|\mathbf{G}\mathbf{h}^{\mathbf{glac}} - \mathbf{h}^{\mathbf{GPR}}\right\| < \boldsymbol{\varepsilon}^{\mathbf{GPR}}$, and the average ice thickness misfits over the entire glacier area $\left(mean\left(\mathbf{h}^{\mathbf{glac}} - \mathbf{h}^{\mathbf{true}}\right)\right)$ ($\mathbf{h}^{\mathbf{true}}$ = “true” model) are 20 m, 25 m and 15 m for the three data sets, respectively. It should be noted that the glaciological models are calibrated with $\alpha_{GPR}$. If no GPR data would have been available, the performance of the glaciological models would be even worse.

Subsequently, it is analyzed which of the profiles *j (j = 1…number of profiles)* causes the largest discrepancies between $\mathbf{h}^{\mathbf{GPR}}$ and $\mathbf{h}^{\mathbf{glac}}$. For that purpose we define

(12) $$d_1^{cost} = \max_j \left( \frac{\sum_{i=1}^{i=n_j} P\left(\left|h_{ij}^{GPR} - h_{ij}^{glac}\right|\right)}{\mathrm{c}_j} \right),$$

The Cryosphere Discuss., https://doi.org/10.5194/tc-2019-55
Manuscript under review for journal The Cryosphere
Discussion started: 25 March 2019


The Cryosphere Discussions
Open Access
EGU

where index $i$ runs over all $n_j$ data points of profile $j$. $h_{ij}^{GPR}$ and $h_{ij}^{glac}$ represent the measured and modelled ice thickness at data point $i$ of profile $j$. The function $P$ is defined as

$$P(x) := \begin{cases} 1 & if\ x > \varepsilon^{GPR} \\ 0 & if\ x \leq \varepsilon^{GPR} \end{cases} . \tag{13}$$

Since longer profiles would be associated with higher (monetary) data acquisition costs, the discrepancy $d_1^{cost}$ is normalized with a cost factor $c_j$, defined as

$$c_j = \max\left(len_j, 200\right) , \tag{14}$$

where $len_j$ represents the length of profile $j$. This cost function assumes that the acquisition costs increase linearly with profile length, which is realistic, because the helicopter costs are typically charged per minute of flight time. To avoid that overly short profiles would dominate $d_1^{cost}$, the assumption was made that profiles with $len$ < 200 m would incur the same costs (for such short profiles the flight time is typically governed by positioning the helicopter at the starting point of a profile).

The profile associated with the largest discrepancy $d_1^{cost}$ is expected to offer the largest amount of additional information per unit cost. In this virtual experiment, we assumed that one would acquire this profile and subsequently perform a GlaTE inversion, yielding an improved model $\mathbf{h}^{\mathrm{est}_k}$. Index $k$ indicates the actual state of the experimental design, that is, $k$ is equal to 1, when adding the first profile. Then, the next profile line to be acquired is identified using

$$d_{k+1}^{cost} = \max_j \left( \frac{\sum_{i=1}^{i=n_j} P\left(\left|h_{ij}^{GPR} - h_{ij}^{est_k}\right|\right)}{\mathrm{c}_j} \right) \tag{15}$$

Repeated application of Equation (15) identifies an optimized sequence for how the profiles should be acquired. Figures 7a, 7c and 7e show the evolution of what we call the "data fit curve", i.e. the evolution of

$$d_{k+1}^{fit} = \max_j \left( \frac{\sum_{i=1}^{i=n_j} \hat{P}\left(\left|h_{ij}^{GPR} - h_{ij}^{est_k}\right|\right)}{n_j} \right) \tag{16}$$

The Cryosphere Discuss., https://doi.org/10.5194/tc-2019-55
Manuscript under review for journal The Cryosphere
Discussion started: 25 March 2019


with

$$\hat{P}(x) := \begin{cases} 0 & \text{if } x > \varepsilon^{GPR} \\ 1 & \text{if } x \le \varepsilon^{GPR} \end{cases} . \quad (17)$$

For the Morteratsch and Plaine Morte data, there is an approximately linear increase of the data fit curve. Likewise, we observe a corresponding linear decrease of the average model misfit. As discussed in Maurer et al. (2010), benefit-cost curves, such as the $\boldsymbol{d}^{fit}$ graphs in Figure 7, typically enter into the area of diminishing returns at some stage, that is, the curves exhibit a characteristic kink and flatten out at larger numbers of profiles. This indicates that it becomes increasingly expensive to obtain additional information. The curves in Figures 7a and 7c therefore indicate that the area of diminishing returns was not reached during the Morteratsch and Plain Morte campaigns, and that it would have been useful to acquire more profiles. In contrast, the $\boldsymbol{d}^{fit}$ and average misfit curves for the Dom region (Figure 7e) start flattening out, although we do not observe a characteristic kink in the curves. This indicates that it would have been very expensive to obtain a more accurate ice thickness distribution for the Dom field site.

The Cryosphere Discuss., https://doi.org/10.5194/tc-2019-55
Manuscript under review for journal The Cryosphere
Discussion started: 25 March 2019


The Cryosphere
Discussions
Open Access

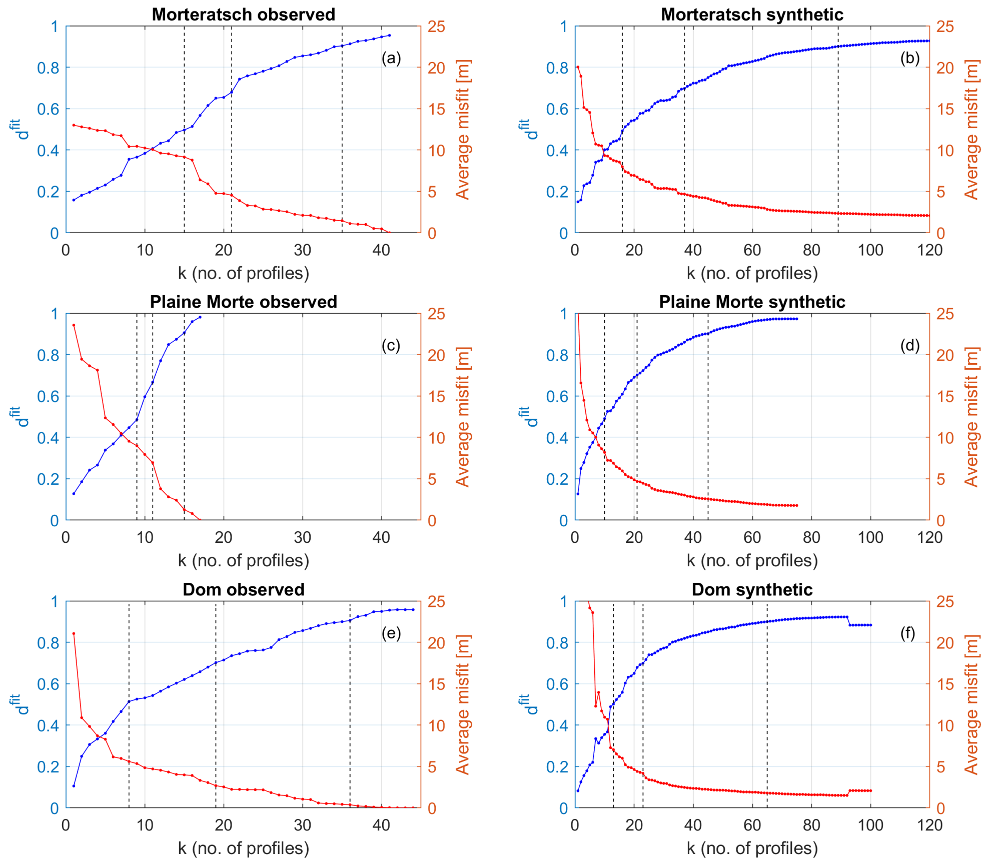


*Figure 7: Evolution of data fit* $\mathbf{d}^{\mathbf{fit}}$ *(blue curves) and average data misfit* $mean\left(\mathbf{h}^{\mathbf{est}_k}-\mathbf{h}^{\mathbf{true}}\right)$ *(red curves). Panels a), c) and e) show the results for the observed data, and panels b), d) and f) show the results for the synthetic data generated on a densely spaced grid of hypothetical profiles . Vertical dashes lines indicate the number of profiles required to achieve* $d^{fit}$ *values of 0.5, 0.7 and 0.9 (see also Figures 8 to 13).*

Figures 8 to 10 show examples of model misfit plots $\left(\mathbf{h}^{\mathbf{est}_k}-\mathbf{h}^{\mathbf{true}}\right)$ superimposed with the selected profile lines. The corresponding stages of the selection procedure are indicated with black dashed lines in Figures 7a, 7c and 7e. For the Morteratschgletscher, profiles are selected preferentially in the western part, because the model fit is already quite good in the eastern region. For Plaine Morte, it is interesting to note that most N-S profiles are selected before the longer and thus more expensive E-W oriented profiles are considered. In the Dom region, no obvious selection patterns can be recognized.

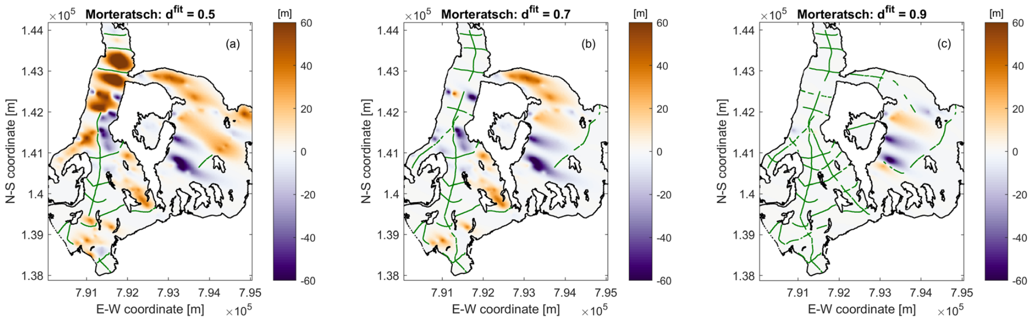


*Figure 8: Morteratsch model misfit* $\mathbf{h}^{true}$ - $\mathbf{h}^{est_k}$ *after selected stages of the experimental design procedure using observed data (see also vertical dashed lines in Figure 7). The selected GPR profiles are superimposed with green lines.*

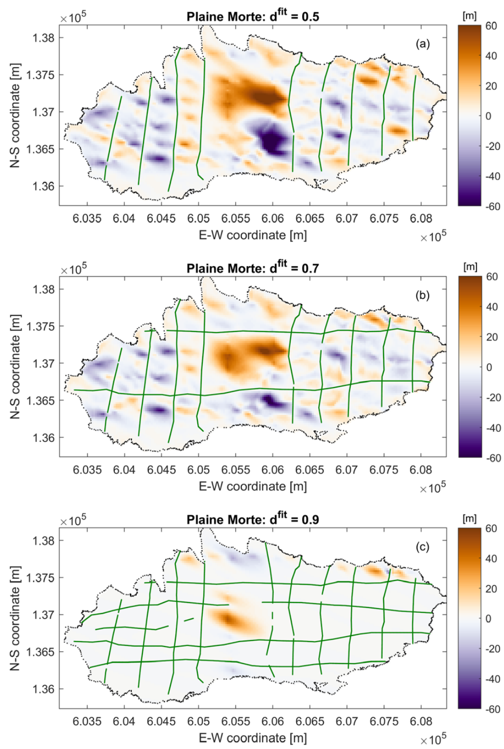


*Figure 9: Plaine Morte model misfit* $\mathbf{h}^{true}$ - $\mathbf{h}^{est_k}$ *after selected stages of the experimental design procedure using observed data (see also vertical dashed lines in Figure 7). The selected GPR profiles are superimposed with green lines.*

The Cryosphere Discuss., https://doi.org/10.5194/tc-2019-55
Manuscript under review for journal The Cryosphere
Discussion started: 25 March 2019


The Cryosphere Discussions
Open Access
EGU

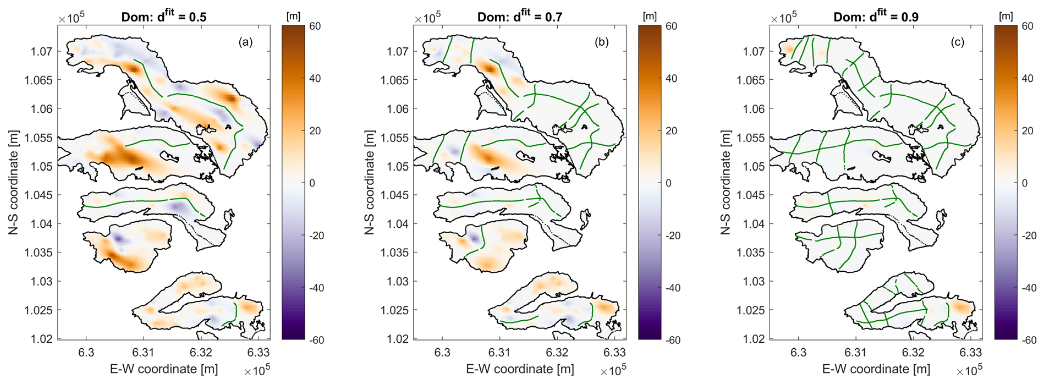


*Figure 10: Dom model misfit* $\mathbf{h}^{\mathbf{true}}$ - $\mathbf{h}^{\mathbf{est}_k}$ *after selected stages of the experimental design procedure using observed data (see also vertical dashed lines in Figure 7). The selected GPR profiles are superimposed with green lines.*

A major limitation of this design experiment is that the "true" model and the recorded GPR profiles have a strong dependency. When all profiles of a particular region are selected, there is a perfect match between $\mathbf{h}^{\mathbf{est}_k}$ and $\mathbf{h}^{\mathbf{true}}$. However, this is the result of our choice of the "true" model, and thus not indicate that this data set is optimal. To reduce, at least partially, this dependency, we have generated synthetic data sets that are covering all glacierized areas with a dense grid. We assumed a line spacing of 100 m and an inline sampling interval of 0.5 m, which is representative for the helicopter-borne GPR data that we acquired. With such a comprehensive data set, the experimental design procedure should have more flexibility to choose cost-optimized suites of profiles.

The resulting benefit-cost curves are shown in Figures 7b, 7d and 7f. As expected, the curves start flattening out after selecting a sufficiently large number of profiles. For the Morteratschgletscher (Figure 7b), it seems to be worthwhile acquiring more than the 43 profiles acquired during the actual experiment. After about 70 profiles, there is no significant benefit observed. Likewise, the curves for the Glacier Plaine Morte (Figure 7d) indicate clearly that acquiring a larger number of profiles would have been beneficial. After adding about 40 profiles, the $\mathbf{d}^{\mathbf{fit}}$ curve starts flattening out. Only for the Dom region, the amount of profiles chosen for the actual survey seems to be adequate (Figure 7f). Note that the decrease in $\mathbf{d}^{\mathbf{fit}}$ at about $k = 8$ and $k = 90$ in Figure 7f are the result of the applied smoothing constraints interfering with the data fit, but this does not affect the general shape of the curve.

Using the $\mathbf{d}^{\mathbf{fit}}$ curves in Figure 7 seems to be a good option for selecting an appropriate number of profiles, but it is also insightful to consider the associated model misfit curves.

Figures 7b, 7d and 7f indicate that the average misfit $\varepsilon^{GPR} = 5m$ is typically reached well before the $\mathbf{d}^{\mathbf{fit}}$ curves start flattening out.

For the experimental design with the synthetic data, Figures 11 to 13 shows examples of model misfit plots $\left(\mathbf{h}^{\mathbf{est}_k} - \mathbf{h}^{\mathbf{true}}\right)$ superimposed with the selected profile lines. In contrast to the selection based on observed data from the Morteratschgletscher (Figure 8), the design based on the dense synthetic grid (Figure 11) yields a better balance of profiles among the eastern and western portions of the glacier. This is the consequence of the larger flexibility of choosing profiles with the dense grid. For the Glacier Plaine Morte (Figure 12), it is interesting to note that exclusively N-S oriented profiles were chosen. In contrast, predominantly E-W oriented profiles were chosen for the Dom region (Figure 13). Both observations are governed primarily by the cost factor $c_j$ in Equation (15).

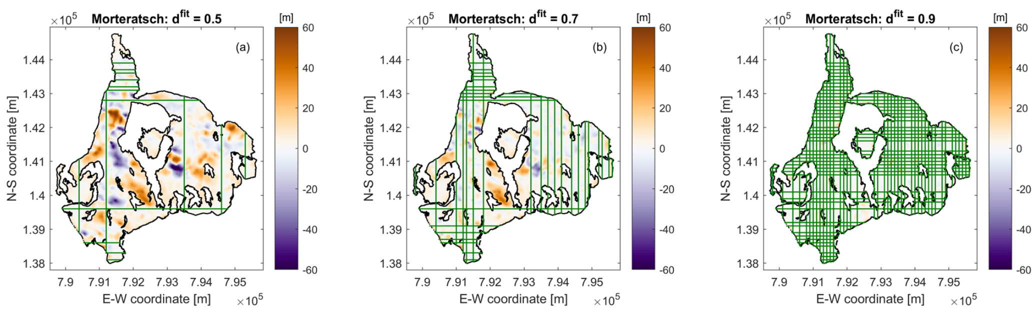


*Figure 11: Morteratschgletscher model misfit* $\mathbf{h}^{\mathbf{true}} - \mathbf{h}^{\mathbf{est}_k}$ *after selected stages of the experimental design procedure using synthetic data (see also vertical dashed lines in Figure 7). The selected GPR profiles are superimposed with green lines.*

The Cryosphere Discuss., https://doi.org/10.5194/tc-2019-55
Manuscript under review for journal The Cryosphere
Discussion started: 25 March 2019

The Cryosphere
Discussions
Open Access

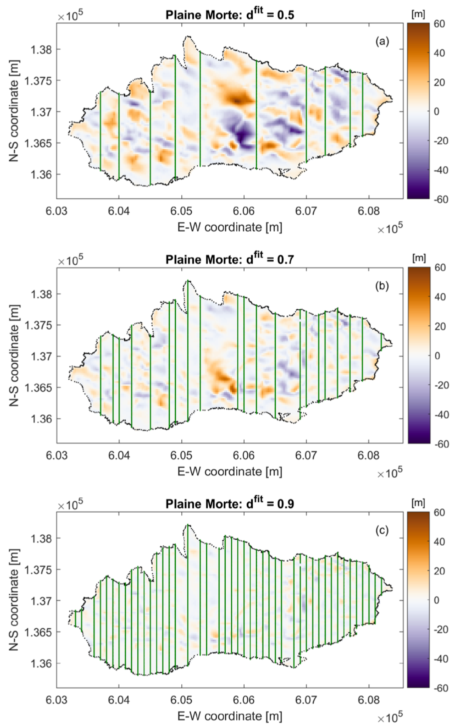


*Figure 12: Glacier Plaine Morte model misfit* $\mathbf{h}^{\mathrm{true}}$ - $\mathbf{h}^{\mathrm{est}_k}$ *after selected stages of the experimental design procedure using synthetic data (see also vertical dashed lines in Figure 7). The selected GPR profiles are superimposed with green lines.*

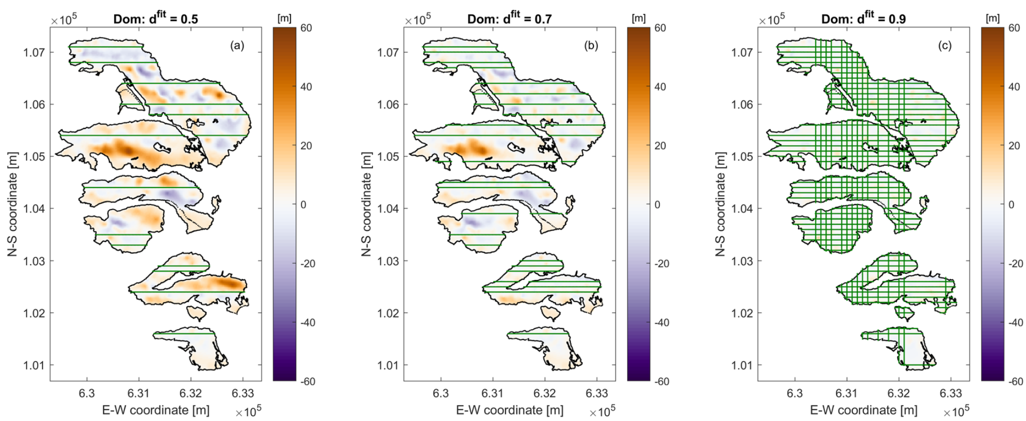


*Figure 13: Dom Region model misfit* $\mathbf{h}^{\mathrm{true}}$ - $\mathbf{h}^{\mathrm{est}_k}$ *after selected stages of the experimental design procedure using synthetic data (see also vertical dashed lines in Figure 7). The selected GPR profiles are superimposed with green lines.*

The Cryosphere Discuss., https://doi.org/10.5194/tc-2019-55
Manuscript under review for journal The Cryosphere
Discussion started: 25 March 2019


## 4 Discussion and conclusions

The GlaTE inversion scheme presented in this paper offers numerous beneficial features. Its main advantage is its versatility, as there are several parameters, by which the algorithm can be tuned to the peculiarities of a particular investigation area. However, this is also one of the method's major drawbacks, since the choice of the control parameters may include a considerable amount of subjectivity. This applies primarily to the choice of the weighting factors $\lambda_1$, $\lambda_2$ and $\lambda_4$. Finding an appropriate value for $\lambda_4$ can be particularly awkward, since there is typically no ground-truth information available on the lateral smoothness of the ice thickness distribution. Therefore, we have chosen to keep $\lambda_1$ and $\lambda_2$ fixed and to determine $\lambda_4$ automatically. Quantifying our (relative) confidence in the GPR constraints ($\lambda_1$) and glaciological constraints ($\lambda_2$) is also a non-trivial task. For this problem, however, some physical arguments may exist. Nevertheless, it might be helpful to repeat the GlaTE inversions with a range of $\lambda_1 / \lambda_2$ ratios and to check the corresponding variations in the resulting models.

Another potential problem is the determination of the scaling factor $\alpha_{GPR}$ in Equation (7). It is largely dependent on the available GPR data, and it is assumed that the GPR profiles have a good areal coverage, which might not be always the case. If values for $\alpha_{GPR}$ would be available for a large number of glaciers, a statistical analysis might be used to correlate the values with specific features of the glaciers (e.g., average steepness, elevation above sea level, size or shape of the glacier, exposure, etc.). This may be helpful in areas, where the GPR data coverage is poor or even non-existent.

In principle, any observations (e.g., boreholes) can be employed as data constraints in Equation (1), but GPR measurements are typically the main source of information. Migration of the GPR data allows the bedrock reflections to be imaged at the correct positions and slopes along a profile, but it is possible that the reflections originated from locations away from the profile lines (off-plane reflections). This may cause systematic errors affecting the reliability of the results. We note, however, that this is not a problem specific to GlaTE, but rather a general issue affecting GPR data acquired on a sparse grid.

As mentioned in Section 2, the system of equations in (11) can be augmented by any linear constraints. An obvious, and in our view particularly useful set of constraints would be offered by surface displacement measurements. They can be obtained from differential satellite images and offer full coverage over a glacier. Such constraints could possibly substitute the smoothness constraints in Equation (11) with a physically more meaningful quantity.

Despite the limitations of our approach, we judge that our results provided useful insights for designing GPR experiments, and some answers to the questions posed in Section 3 can be provided.

The Cryosphere Discuss., https://doi.org/10.5194/tc-2019-55
Manuscript under review for journal The Cryosphere
Discussion started: 25 March 2019


1. *Was the experimental geometry and the amount of data acquired in the three investigation areas adequate?*

   The benefit-cost curves in Figure 7 indicate that, at least for the Morteratsch and Glacier Plaine Morte, it would have been useful to acquire more data.

2. *Do better experimental layouts exist for constraining the ice thicknesses in a cost-optimized manner?*

   The experimental layouts in Figures 8 to 13 do not provide unexpected features, but indicate that acquiring a larger number of shorter profiles, instead of recording a few long ones, could be beneficial, but it should be noted that we do not take into account the flight time required to move to the next profiles. This could be significant on glaciers with steep mountain flanks.

3. *Can some general recommendations for designing helicopter-borne GPR surveys on glaciers be made?*

   Based on our results, it is difficult to offer general recommendations. For estimating the overall amount of data to be collected, the benefit-cost curves are most indicative. However, in our case studies they do not flatten out clearly, thereby indicating that it would be worthwhile acquiring more data. When high-precision ice thickness maps are required, it is therefore advisable to acquire as much data as can be afforded.

   It is common practice to acquire crossing profiles, but from the experimental layouts, shown in Figure 12, it could be concluded that it is not necessary to acquire a large amount of crossing profiles. From a practical point of view, this recommendation cannot be fully supported. When the signal-to-noise ratio of the GPR profiles is poor, it can be difficult to identify the bedrock reflections unambiguously.

   It is not realistic to adopt a real-time experimental design strategy (i.e., choosing the next profile based on the results of the previously acquired data), as assumed in our virtual experiments in Section 3. However, if logistically feasible, it might be useful to employ a two-step acquisition strategy. Initially, only a few profiles could be acquired. After analyzing these data sets, regions, where large discrepancies between $\mathbf{h}^{est}$ and $\mathbf{h}^{glac}$ exist, could be identified, and a suitable set of additional profiles could be acquired with a second campaign.

The Cryosphere Discuss., https://doi.org/10.5194/tc-2019-55
Manuscript under review for journal The Cryosphere
Discussion started: 25 March 2019


## Acknowledgments

We thank Patrick Lathion, Philipp Schaer and Kevin Délèze from GEOSAT SA, Patrick Fauchère from Air Glacier, Hansueli Bärfuss from Heli-Bernina, as well as Lasse Rabenstein and Lino Schmid for acquiring the data. Furthermore, we thank Matthias Huss for fruitful discussions and Daniel Farinotti for an insightful in-house review, which improved the clarity of the manuscript. Financial support was provided by ETH Zurich (Grant ETH-15 13-2), the Innosuisse program SCCER-SOE (Swiss competence center for energy research, supply of electricity), and the Swiss Geophysical Commission and ETH Zurich.

## References

Clarke, G. K., Anslow, F. S., Jarosch, A. H., Radić, V., Menounos, B., Bolch, T., and Berthier, E.: Ice volume and subglacial topography for western Canadian glaciers from mass balance fields, thinning rates, and a bed stress model, J Climate, 26, 4282-4303, 2013.

Constable, S. C., Parker, R. L., and Constable, C. G.: Occam's inversion: A practical algorithm for generating smooth models from electromagnetic sounding data, Geophysics, 52, 289-300, 1987.

Evans, S.: Radio techniques for the measurement of ice thickness, Polar Record, 11, 406-410, 1963.

Farinotti, D., Huss, M., Bauder, A., Funk, M., and Truffer, M.: A method to estimate the ice volume and ice-thickness distribution of alpine glaciers, J Glaciol, 55, 422-430, 2009.

Farinotti, D., Brinkerhoff, D. J., Clarke, G. K., Fürst, J. J., Frey, H., Gantayat, P., Gillet-Chaulet, F., Girard, C., Huss, M., and Leclercq, P. W.: How accurate are estimates of glacier ice thickness? Results from ITMIX, the Ice Thickness Models Intercomparison eXperiment, Cryosphere, 11, 949-970, 2017.

Grab, M., Bauder, A., Ammann, F., Langhammer, L., Hellmann, S., Church, G., Schmid, L., Rabenstein, L., and Maurer, H.: Ice volume estimates of Swiss glaciers using helicopter-borne GPR—an example from the Glacier de la Plaine Morte, 2018 17th International Conference on Ground Penetrating Radar (GPR), 2018, 1-4,

Huss, M., and Farinotti, D.: Distributed ice thickness and volume of all glaciers around the globe, Journal of Geophysical Research: Earth Surface, 117, 2012.

Huss, M., Voinesco, A., and Hoelzle, M.: Implications of climate change on Glacier de la Plaine Morte, Switzerland, Geographica Helvetica, 68, 227-237, 2013.

Iken, A.: Adaption of the hot-water-drilling method for drilling to great depth, Mitteilungen der Versuchsanstalt fur Wasserbau, Hydrologie und Glaziologie an der Eidgenossischen Technischen Hochschule Zurich, 211-229, 1988.

Kamb, B., and Echelmeyer, K. A.: Stress-gradient coupling in glacier flow: I. Longitudinal averaging of the influence of ice thickness and surface slope, J Glaciol, 32, 267-284, 1986.

Langhammer, L., Rabenstein, L., Schmid, L., Bauder, A., Grab, M., Schaer, P., and Maurer, H.: Glacier bed surveying with helicopter-borne dual-polarization ground-penetrating radar, J Glaciol, 1-13, 10.1017/jog.2018.99, 2018.

The Cryosphere Discuss., https://doi.org/10.5194/tc-2019-55
Manuscript under review for journal The Cryosphere
Discussion started: 25 March 2019


Linsbauer, A., Paul, F., and Haeberli, W.: Modeling glacier thickness distribution and bed topography over entire mountain ranges with GlabTop: Application of a fast and robust approach, Journal of Geophysical Research: Earth Surface, 117, 2012.

Maurer, H., Curtis, A., and Boerner, D. E.: Recent advances in optimized geophysical survey design, Geophysics, 75, 75A177 – 175A194, 2010.

Maurer, H., Nuber, A., Martiartu, N. K., Reiser, F., Boehm, C., Manukyan, E., Schmelzbach, C., and Fichtner, A.: Optimized Experimental Design in the Context of Seismic Full Waveform Inversion and Seismic Waveform Imaging, in: Advances in Geophysics, Elsevier, 1-45, 2017.

Menke, W.: Geophysical data analysis : discrete inverse theory, Matlab ed., Academic Press, Waltham, MA, 293 p. pp., 2012.

Morlighem, M., Rignot, E., Seroussi, H., Larour, E., Ben Dhia, H., and Aubry, D.: A mass conservation approach for mapping glacier ice thickness, Geophys Res Lett, 38, 2011.

Morlighem, M., Rignot, E., Mouginot, J., Seroussi, H., and Larour, E.: High-resolution ice-thickness mapping in South Greenland, Annals of Glaciology, 55, 64-70, 2014.

Nye, J.: A method of calculating the thicknesses of the ice-sheets, Nature, 169, 529-530, 1952.

Paige, C. C., and Saunders, M. A.: Lsqr - an Algorithm for Sparse Linear-Equations and Sparse Least-Squares, Acm T Math Software, 8, 43-71, 1982.

Rutishauser, A., Maurer, H., and Bauder, A.: Helicopter-borne ground-penetrating radar investigations on temperate alpine glaciers: A comparison of different systems and their abilities for bedrock mapping, GEOPHYSICS, 81, WA119-WA129, doi:10.1190/geo2015-0144.1, 2016.

Steinhage, D., Nixdorf, U., Meyer, U., and Miller, H.: New maps of the ice thickness and subglacial topography in Dronning Maud Land, Antarctica, determined by means of airborne radio-echo sounding, Annals of Glaciology, 29, 267-272, 1999.

Vermeer, G. J.: 3d seismic survey design optimization, The Leading Edge, 22, 934-941, 2003.

Watts, R. D., and England, A. W.: Radio-echo sounding of temperate glaciers: ice properties and sounder design criteria, J Glaciol, 17, 39-48, 1976.

Zekollari, H., Huybrechts, P., Fürst, J., Rybak, O., and Eisen, O.: Calibration of a higher-order 3-D ice-flow model of the Morteratsch glacier complex, Engadin, Switzerland, Annals of Glaciology, 54, 343-351, 2013.